

## Doubly-resonant sum-frequency generation spectroscopy for surface studies

M.B. Raschke<sup>a,b,\*</sup>, M. Hayashi<sup>c</sup>, S.H. Lin<sup>d</sup>, Y.R. Shen<sup>a,b</sup>

<sup>a</sup> Department of Physics, University of California at Berkeley, Berkeley, CA 94720, USA

<sup>b</sup> Materials Sciences Division, Lawrence Berkeley National Laboratory, Berkeley, CA 94720, USA

<sup>c</sup> Center for Condensed Matter Sciences, National Taiwan University, Taipei, Taiwan, ROC

<sup>d</sup> Institute of Atomic and Molecular Sciences, Academia Sinica, Taipei, Taiwan, ROC

Received 17 October 2001; in final form 4 January 2002

### Abstract

Doubly-resonant infrared–visible sum-frequency generation (DR-SFG) as a two-dimensional surface spectroscopy was demonstrated experimentally for the first time. Probing electronic and vibrational transitions of a surface molecular monolayer simultaneously, the technique gives access to information about the electron-vibration coupling of the surface molecules. It allows selective studies of any interface accessible by light. © 2002 Elsevier Science B.V. All rights reserved.

Second-harmonic and sum-frequency generation (SHG/SFG) have found a wide range of applications as probes in surface science due to their intrinsic surface and interface sensitivity and specificity [1–5]. In particular, infrared–visible SFG has emerged as a versatile spectroscopic technique applicable to such diverse systems as polymer, semiconductor and metal surfaces, heterogeneous catalysis, electrochemistry and liquid interfaces. In this process, two input beams, one visible at  $\omega_{\text{vis}}$  and the other infrared at  $\omega_{\text{IR}}$ , overlap on the surface of the material being investi-

gated and the sum-frequency generation, typically in reflection, at  $\omega_s = \omega_{\text{vis}} + \omega_{\text{IR}}$  is detected. When  $\omega_{\text{IR}}$  is tuned over vibrational resonances the SF output exhibits resonant enhancement. The observed vibrational spectrum provides information about surface composition and structure, as well as surface dynamical properties via time-dependent measurements.

With both  $\omega_{\text{IR}}$  and  $\omega_{\text{vis}}$  near surface vibrational and electronic transitions, respectively, SFG could be doubly resonantly enhanced [6]. In this respect it is similar to resonance Raman spectroscopy (RRS), known for its applications in condensed matter physics, chemistry, and biology, but SFG has the additional virtue of being surface-specific. Analogous to RRS, doubly resonant (DR) enhancement in SFG occurs when the corresponding vibrational and electronic transitions are coupled.

\* Corresponding author. Present address: Max-Born-Institut, D-12489 Berlin, Germany. Fax: +49-(0)30-63921489.

E-mail addresses: [raschke@mbi-berlin.de](mailto:raschke@mbi-berlin.de) (M.B. Raschke), [shenyr@socrates.berkeley.edu](mailto:shenyr@socrates.berkeley.edu) (Y.R. Shen).

This allows for more selective spectroscopic information and better assignment of the surface modes. It permits deduction of the coupling strengths between various electronic and vibrational transitions. The new technique could also be valuable for studies of inter-molecular interactions at surfaces and interfaces.

Here we report the first experiment on DR-SFG. While the technique is generally applicable to any interface accessible by light, including those between two pure media, we used adsorbed monolayers of Rhodamine 6G (Rh6G) as an example to demonstrate the principles of this technique. Doubly resonant enhancement from coupled electronic and vibrational transitions of Rh6G was observed. It exhibited an unprecedented surface sensitivity. From the DR-SFG spectra, relative electron–vibration coupling strengths between different vibrational modes and the  $S_0$ – $S_1$  electronic resonance of Rh6G were deduced.

We first briefly describe the theory of DR-SFG. In the electric-dipole approximation, surface SFG from a material with inversion symmetry arises from the second-order polarization

$$\mathbf{P}^{(2)}(\omega_s = \omega_{\text{vis}} + \omega_{\text{IR}}) = \epsilon_0 \chi^{(2)}(\omega_s) : \mathbf{E}(\omega_{\text{vis}}) \mathbf{E}(\omega_{\text{IR}}) \quad (1)$$

induced by the input fields  $\mathbf{E}(\omega_{\text{vis}})$  and  $\mathbf{E}(\omega_{\text{IR}})$  at the surface, where  $\chi^{(2)}$  denotes the second-order surface nonlinear susceptibility tensor<sup>1</sup> [7,8]. In the infrared–visible (and visible–infrared) DR-SFG process shown schematically in Fig. 1, the microscopic expression for  $\chi^{(2)}$  is dominated by doubly resonant terms [6,9,10]. As will be discussed later, the visible–infrared DR-SFG is much weaker and not detected in our experiment because of the very fast relaxation of the electronic excitation. Therefore here only the IR–visible DR-SFG process is considered. One finds, at temperature  $T = 0$  K,

$$\chi_{ijk}^{(2)} = -\frac{N}{\hbar^2} \left\langle \sum_{b,n} \frac{\langle \psi_{g0} | \mu_i | \psi_{en} \rangle \langle \psi_{en} | \mu_j | \psi_{gb} \rangle \langle \psi_{gb} | \mu_k | \psi_{g0} \rangle}{(\omega_s - \omega_{en,g0} + i\Gamma_{en,g0})(\omega_{\text{IR}} - \omega_{gb,g0} + i\Gamma_{gb,g0})} \right\rangle + (\chi_{\text{NR}}^{(2)})_{ijk}, \quad (2)$$

<sup>1</sup> We use MKS units and follow the convention of separating  $\epsilon_0$  from  $\chi$ .

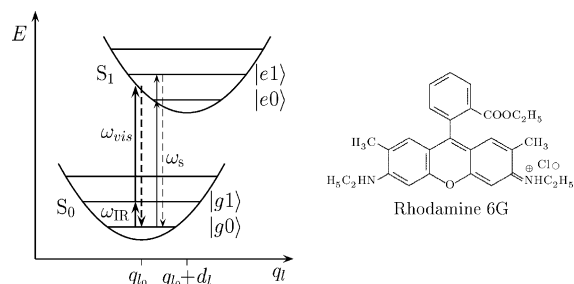


Fig. 1. Model adiabatic potentials for molecular electronic ground and excited states as functions of configurational coordinate  $q_l$ . The resonant transitions involved in the doubly resonant IR–visible (and visible–IR) sum-frequency generation processes are shown schematically.

where  $N$  is the surface molecular density,  $\mu$  the electric-dipole operator, and  $b$ ,  $n$ , and  $g$ ,  $e$  label vibrational and electronic states, respectively.  $\omega_{en,g0}$ ,  $\omega_{gb,g0}$ , and  $\Gamma_{en,g0}$ ,  $\Gamma_{gb,g0}$  denote transition frequencies and damping constants, respectively, the angular brackets represent an average over molecular orientations, and  $(\chi_{\text{NR}}^{(2)})_{ijk}$  describes the more weakly dispersive contributions that include singly resonant terms and the visible–IR double resonances. Under the Born–Oppenheimer approximation,  $\langle \psi_{gb} | \mu_k | \psi_{g0} \rangle \simeq \sum_l (\partial \mu_{gg}^k / \partial q_l) \langle gb | q_l | g0 \rangle$  Eq. (2) becomes

$$\chi_{ijk}^{(2)} = -\frac{N}{\hbar^2} \left\langle \sum_{b,n} \sum_l \mu_{ge}^i \mu_{eg}^j \frac{\partial \mu_{gg}^k}{\partial q_l} \frac{\langle g0 | en \rangle \langle en | gb \rangle \langle gb | q_l | g0 \rangle}{(\omega_s - \omega_{en,g0} + i\Gamma_{en,g0})(\omega_{\text{IR}} - \omega_{gb,g0} + i\Gamma_{gb,g0})} \right\rangle + (\chi_{\text{NR}}^{(2)})_{ijk}, \quad (3)$$

where the subindex  $l$  denotes the  $l$ th vibrational mode.

In this Letter, for explicit evaluation of Eq. (3), we use a simple model to describe the states involved in the DR process [6]. Each vibrational mode is treated as a harmonic oscillator linearly coupled with the electronic ground and excited states,  $|g\rangle$  and  $|e\rangle$ . The electron–vibration coupling then results in a reduced-mass weighted displacement  $d_l$  between the two vibrational potential energy curves  $E_g(q_l)$  and  $E_e(q_l)$  along the vibrational

coordinate  $q$  (see Fig. 1) with  $d_l = a_l \sqrt{\hbar/\omega_l}$  (with dimension (distance) $\sqrt{\text{mass}}$  where  $a_l$  is the dimensionless Franck–Condon electron–vibration coupling coefficient and  $\omega_l$  the frequency of the  $l$ th vibrational mode. For simplicity we assume that the vibrational mode frequencies remain the same for the electronic ground and excited states, but this assumption, as well as the assumption of linear electron–vibration coupling, can be relaxed readily [9,11]. The vibrational wavefunctions associated with the electronic ground and excited states are then given by the eigenfunctions of a harmonic oscillator in the appropriate normal coordinates,  $\phi_v(q_l)$  and  $\phi_u(q_l + d_l)$  for  $|gv\rangle$  and  $|eu\rangle$ , respectively. Consequently, the matrix elements in the summation of Eq. (3) can be derived explicitly. Here, we focus on one vibrational mode at a time, and neglected that all vibrational modes should participate simultaneously in the process. The more complete calculation involving all vibrational modes will be published elsewhere. We obtain from this simple model [12]

$$\chi_{ijk}^{(2)} = \sum_l (\chi_{ijk}^{(2)})_l + (\chi_{NR}^{(2)})_{ijk},$$

$$(\chi_{ijk}^{(2)})_l = -\frac{N}{\hbar^2} \left\langle \mu_{eg}^i \mu_{ge}^j \frac{\partial \mu_{gg}^k}{\partial q_l} \frac{\sqrt{S_l} e^{-S_l}}{\omega_{IR} - \omega_l + i\Gamma_l} \right.$$

$$\times \sum_{n=0}^{\infty} \frac{S_l^n}{n!} \left\{ \frac{1}{\omega_s - n\omega_l - \omega_{eg} + i\Gamma_{en,g0}} \right.$$

$$\left. \left. - \frac{1}{\omega_s - (n+1)\omega_l - \omega_{eg} + i\Gamma_{en+1,g0}} \right\} \right\rangle, \quad (4)$$

where  $S_l = d_l^2 \omega_l / 2\hbar$ , known as the Huang–Rhys factor, is related to  $a_l$  by  $S_l = a_l^2 / 2$ . We shall use Eq. (4) to fit the experimental DR-SFG spectra and deduce the coupling strengths  $S_l$  in the data analysis.

In our experiment, we used a homogeneous monolayer of Rhodamine 6G dye molecules on a fused silica substrate as a representative system. Rh6G was chosen because its spectral characteristics are well understood from extensive spectroscopic studies in the past [13–18]. The samples were prepared by spin-coating a 0.3 mM ethanolic solution resulting in a surface molecular density of

$3 \times 10^{13} \text{ cm}^{-2}$ , as determined by visible absorption measurements.

For the DR-SFG experiments, tunable IR and visible light was provided by two optical parametric generator/amplifier systems pumped by a Nd:YAG laser with an 18 ps pulsewidth and a 20 Hz repetition rate [19]. The two input pulses were overlapped on the sample with incident angles of  $\beta_{IR} = 40^\circ$  and  $\beta_{vis} = 50^\circ$ . The SFG output was detected in the reflected direction after spatial and spectral filtering. The combined maximum input fluence on the sample was limited to  $100 \text{ mJ/cm}^2$  off the Rh6G  $S_0$ – $S_1$  absorption band and to  $20 \text{ mJ/cm}^2$  near it to avoid laser heating or photo-induced reactions. The SFG spectra were reproducible within 20% from measurements on different samples. The SFG output was normalized against that from a z-cut quartz crystal allowing for the determination of absolute values of  $|\chi_{ijk}^{(2)}|$ .

DR-SFG spectroscopy was performed by tuning  $\omega_{IR}$  over vibrational resonances of Rh6G in the  $1500$ – $1750 \text{ cm}^{-1}$  range and keeping  $\omega_{vis}$  fixed at different values. The visible frequencies  $\omega_{vis}$  were chosen such that they cover the  $S_0$ – $S_1$  absorption peak. A representative set of spectra obtained with the ssp (s-, s-, and p-polarizations for SF, visible, and IR fields, respectively) polarization combination is shown in Fig. 2. In each spectrum four distinct peaks appear. Those at  $1514$ ,  $1573$ , and  $1657 \text{ cm}^{-1}$  can be attributed to the xanthen skeleton vibrational modes of Rh6G and the one at  $1614 \text{ cm}^{-1}$  to the phenyl group attached to the xanthen [16,17]. All of them exhibit a pronounced variation in their peak intensities as  $\omega_{vis}$  is varied. The maximum value of  $\chi^{(2)}$  at the peak of the  $1657 \text{ cm}^{-1}$  resonance is  $\sim 4.7 \times 10^{-20} \text{ m}^2/\text{V}$  as compared to  $\sim 7 \times 10^{-22} \text{ m}^2/\text{V}$  for a stretch mode of a typical CH-group of equivalent surface density measured by conventional singly resonant SFG.

To analyze the spectra, we note that with the visible input frequency  $\omega_{vis}$  fixed, Eq. (3) or (4) can be approximated by the form

$$\chi_{ijk}^{(2)} = \sum_l \frac{A_l}{\omega_{IR} - \omega_l + i\Gamma_l} + \chi_{NR,ijk}^{(2)}. \quad (5)$$

We use Eq. (5) to fit all the measured spectra with  $\omega_l$ ,  $\Gamma_l$ ,  $A_l$  and  $\chi_{NR}^{(2)}$  as adjustable parameters. For

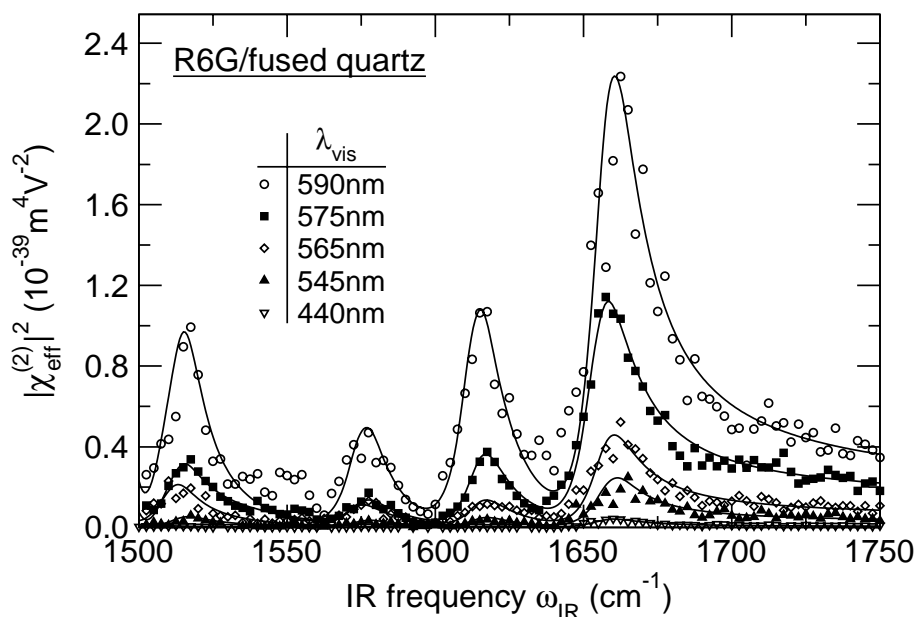


Fig. 2. Doubly resonant sum-frequency spectra of a molecular monolayer of Rhodamine 6G molecules on fused quartz in ssp polarization combination normalized against the signal from a z-cut quartz. The solid lines were derived from a numerical fit using Eq. (5).

each vibrational mode,  $\omega_l$  and  $\Gamma_l$  are taken as independent of  $\omega_s$ , but  $A_l$  and  $\chi_{\text{NR}}^{(2)}$  do vary with  $\omega_s$ . The results are displayed in Fig. 3, where  $|A_l|$  is plotted versus  $\omega_s$  for three vibrational modes. We refer to these curves as the excitation spectra for the DR-SFG process involving the vibrational modes. As expected, all the excitation spectra exhibit a resonance coincident with the  $S_0$ – $S_1$  linear absorption peak for the Rh6G monolayer, which is plotted for comparison.

It can be seen that the absorption peak in Fig. 3 shows a longer tail on the high-frequency side than the peak in the excitation spectra. This is due to contributions from vibronic transitions involving coupled vibrational modes in the absorption. One would expect these transitions to also contribute to the excitation spectra of DR-SFG: In Eq. (4) there are successive resonant terms describing  $\omega_s$  in resonance with vibronic transitions with frequencies  $\omega_{eg} + n\omega_l$  for  $n = 0, 1, 2$ , etc. Although their amplitude drops off rapidly with increasing  $n > 1$ , for small electron–vibration coupling one would expect to see the  $n = 1$  vibrational sideband in the excitation spectrum (see also below). This, how-

ever, was not clearly observed in our experiment and could be due to fact that the vibronic transitions of Rh6G have significantly shorter dephasing times [14]. The corresponding larger damping constants ( $\Gamma_{en,g0}$  in Eq. (4)) or spectral widths would then suppress the resonant contributions, with respect to  $\chi_{\text{NR}}^{(2)}$  in Eq. (5), below the discernible level.

We can deduce an explicit expression for  $A_l(\omega_s)$  by comparing Eq. (4) with Eq. (5). To fit the observed excitation spectra, we use, for each vibrational mode  $q_l$ ,  $S_l$  and  $\Gamma_{en,g0}$  as adjustable parameters. The zero-vibration  $S_0$ – $S_1$  transition frequency,  $\omega_{eg}$ , is taken as  $18400 \text{ cm}^{-1}$  (2.28 eV). We find that a good description of the observed excitation spectrum for the  $1657 \text{ cm}^{-1}$  mode requires  $\Gamma_{e0,g0} = (500 \pm 50) \text{ cm}^{-1}$  and  $\Gamma_{en,g0} = (2 \pm 0.4)\Gamma_{e0,g0}$  for  $n \geq 1$  (Fig. 3a, solid line). For comparison, using  $\Gamma_{en,g0} = \Gamma_{e0,g0}$  while keeping all other parameters fixed, we obtain the dashed curve for  $A_l(\omega_s)$ . The other three vibrational modes, require  $\Gamma_{e0,g0} = (500 \pm 50) \text{ cm}^{-1}$  and  $\Gamma_{en,g0} \gtrsim 3\Gamma_{e0,g0}$  for  $n \geq 1$  to fit the experimental data (Fig. 3b). These results indicate that the vibronic transitions

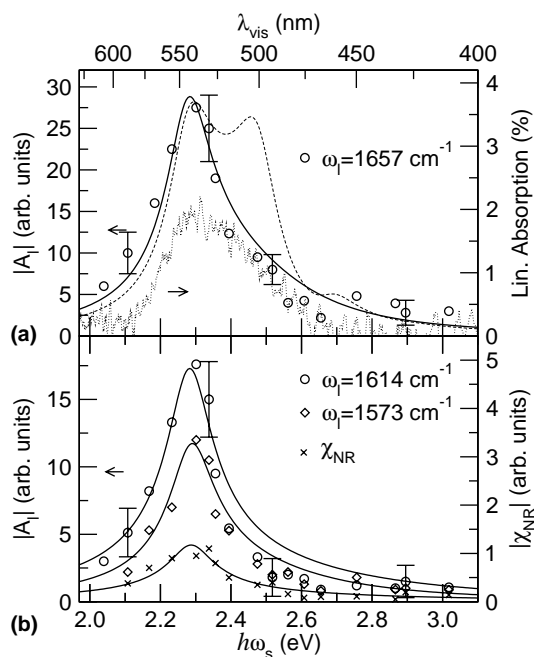


Fig. 3. Excitation spectra of DR-SFG for three vibrational modes of Rh6G plotted as a function of the sum-frequency photon energy (open symbols) in comparison with the linear absorption spectrum (dots). The solid and dashed lines are numerical fits using the model described in the text.

have shorter dephasing times than the zero-vibronic transition. Early measurements found that the dephasing times of vibronic transitions of Rh6G are less than 30 fs [14]. The larger  $\Gamma_{en,g0}$  will also suppress the resonant enhancement of DR-SFG that starts with an electronic transition followed by a vibrational transition in the electronic excited state (see Fig. 1). Since this process was not observed it has been neglected in the derivation of Eqs. (3) and (4).

Without being able to resolve the vibronic sidebands in our excitation spectra, except for setting an upper limit of  $S \sim 0.2$  for the 1657  $\text{cm}^{-1}$  mode, we cannot determine the absolute values of  $S$  for the vibrational modes of Rh6G. We can, however, obtain relative values of  $S$ , using relative values of  $\partial\mu_{gg}/\partial q_l$  in Eq. (4) for the different modes. The latter were deduced from an infrared absorption measurement of Rh6G dissolved in solid KBr and are summarized in

Table 1

Result of best fit to the DR-SFG experimental data from calculations described in the text.  $\partial\mu_{gg}/\partial q_l$  denotes relative infrared vibrational intensities. The parameter  $S_{\text{rel}}$  refers to the relative electron–vibration coupling constant.

$\omega_{g1,g0}$ ( $\text{cm}^{-1}$ )	$\Gamma_{g1,g0}$ ( $\text{cm}^{-1}$ )	$\partial\mu_{gg}/\partial q_l$	$S_{\text{rel}}$
1514	8	4.5	0.02
1573	8	0.8	0.25
1614	8	7.5	0.005
1657	9	1.0	1.0

$\omega_{e0,g0}$ ( $\text{cm}^{-1}$ )	$\Gamma_{e0,g0}$ ( $\text{cm}^{-1}$ )	$\Gamma_{en(n \geq 1),g0}$ ( $\text{cm}^{-1}$ )
18 400	500	1000–1500

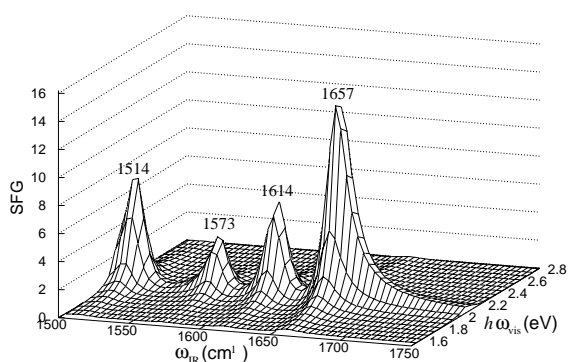


Fig. 4. Simulated DR-SFG spectrum of Rh6G using the parameters given in Table 1.

Table 1 together with the resulting values for  $S_{\text{rel}}$ . Fig. 4 then presents the calculated two-dimensional DR-SFG spectrum using these tabulated parameters.

For Rh6G, the  $S_0$ – $S_1$  electronic transition is dominated by the  $\pi$ – $\pi^*$  excitation of the large xanthene group of the molecule. As mentioned earlier the vibrational mode at 1614  $\text{cm}^{-1}$  can be assigned to the pendant phenyl group while those at 1514, 1573 and 1657  $\text{cm}^{-1}$  directly to the xanthene group. They are expected to have different degrees of coupling with the electronic transition. In agreement with the results from resonance Raman experiments from Rh6G in solution [16–18] the 1614  $\text{cm}^{-1}$  mode has the smallest coupling strength because the phenyl ring is external to the xanthene group and is rotated out of

the molecular plane. Despite the small coupling strength, the mode still has the strongest peak intensity in the SFG spectra since it has the largest IR absorption strength of all vibrational modes of Rh6G.

In summary, we have performed the first DR-SFG experiment and shown that it is a viable two-dimensional surface spectroscopic technique. In much the same way as multi-dimensional spectroscopy is suitable for studies of intra- and inter-molecular interactions in the bulk, DR-SFG provides a similar opportunity for studies of molecules at surfaces. In our experiment, the doubly resonant enhancement allowed deduction of coupling between electronic transitions and vibrational modes. Although the experiment reported here is on adsorbed molecular monolayer, the technique can be extended to studies of interaction between any pairs of surface resonances and is applicable to all surfaces and interfaces accessible by light, including those of neat liquids and solids.

### Acknowledgements

The authors acknowledge valuable discussions with J. McGuire and X. Wei. This work was supported by the Director, Office of Energy Research, Office of Basic Energy Sciences, Materials Science Division of the US Department of Energy under Contract No. DE-AC03-76SF00098, and a Max-Planck Society Research Award. SHL and MH thank the NSC of ROC and Academia Sinica, and MBR thanks the Alexander von Humboldt Foundation and the Max-Planck Society for financial support.

### References

- [1] T.F. Heinz, in: H.-E. Ponath, G.I. Stegeman (Eds.), *Nonlinear Surface Electromagnetic Phenomena*, North-Holland, Amsterdam, 1991, p. 353.
- [2] Y.R. Shen, in: T.W. Hänsch, M. Inguscio (Eds.), *Frontiers in Laser Spectroscopy*, North-Holland, Amsterdam, 1994, p. 139.
- [3] P. Guyot-Sionnest, A.L. Harris, in: H.-L. Dai, W. Ho (Eds.), *Laser Spectroscopy and Photochemistry on Metal Surfaces*, World Scientific, Singapore, 1995; J.Y. Huang, Y.R. Shen, in: H.-L. Dai, W. Ho (Eds.), *Laser Spectroscopy and Photochemistry on Metal Surfaces*, World Scientific, Singapore, 1995.
- [4] P. Dumas, M.K. Weldon, Y.J. Chabal, G.P. Williams, *Surf. Rev. Lett.* 6 (1999) 225.
- [5] E. Matthias, F. Träger (Eds.), *Appl. Phys. B, Nonlinear Optics at Interfaces* 210 (3) (1999) (special issue).
- [6] J.Y. Huang, Y.R. Shen, *Phys. Rev. A* 49 (1994) 3973.
- [7] N. Bloembergen, *Nonlinear Optics*, Benjamin, New York, 1977.
- [8] Y.R. Shen, *The Principles of Nonlinear Optics*, Wiley, New York, 1984.
- [9] J.C. Vallet, A.J. Boeglin, J.P. Lavoine, A.A. Villaeys, *Phys. Rev. A* 53 (1996) 4508.
- [10] S.H. Lin, M. Hayashi, R. Islampour, J. Yu, D.Y. Yang, G.Y.C. Wu, *Physics B* 222 (1996) 191.
- [11] R. Islampour, M. Hayashi, S.H. Lin, *Chem. Phys. Lett.* 234 (1995) 7.
- [12] E. Hutchisson, *Phys. Rev.* 36 (1930) 410; H. Kuzmany, *Solid-state Spectroscopy*, Springer, Berlin, 1998.
- [13] T.F. Heinz, C.K. Chen, D. Ricard, Y.R. Shen, *Phys. Rev. Lett.* 48 (1982) 478.
- [14] C.V. Shank, E.P. Ippen, O. Teschke, *Chem. Phys. Lett.* 45 (1977) 291.
- [15] A.J. Taylor, D.J. Erskine, C.L. Tang, *Chem. Phys. Lett.* 103 (1984) 430.
- [16] P. Hildebrandt, M. Stockburger, *J. Phys. Chem.* 88 (1984) 5935.
- [17] M. Majoube, M. Henry, *Spectrochim. Acta* 47 (1991) 1459.
- [18] M. Takayanagi, H. Hamaguchi, M. Tasumi, *Chem. Phys. Lett.* 128 (1986) 555.
- [19] J.Y. Zhang, J.Y. Huang, Y.R. Shen, C. Chen, *J. Opt. Soc. Am. B* 10 (1993) 1758.